




# Magnetometer-Based Attitude Determination Extended Kalman Filter and Optimization Techniques

SUPAKIT WATTANARUNGSAN   
TOSHINORI KUWAHARA , Member, IEEE  
SHINYA FUJITA   
Tohoku University, Sendai, Japan

Magnetometer-based attitude determination algorithm has been studied for decades owing to its advantages. This article aims to develop and fine-tune the magnetometer-based attitude determination method by introducing two new observation models for the extended Kalman filter (EKF). The optimization techniques were purposed to increase accuracy and improve convergence. The Monte Carlo simulation, including disturbances and a moment of inertia estimation error, was held to evaluate the performance of each EKF by the innovation vector and convergence. The significant effect of singularity on the reliability of the estimator was discovered and resolved by optimization. The study concluded that the attitude representation observation EKF with optimizations reduced the convergence time and provided reliability.

Manuscript received 7 October 2022; revised 1 February 2023 and 3 May 2023; accepted 17 July 2023. Date of publication 31 July 2023; date of current version 8 December 2023.

DOI. No. 10.1109/TAES.2023.3299897

Refereeing of this contribution was handled by Jiwon Seo.

Authors' addresses: Supakit Wattanarungsan, Toshinori Kuwahara, and Shinya Fujita are with the Department of Aerospace Engineering, Tohoku University, Sendai 980-0812, Japan, E-mail: (wattanarungsan.supakit.r3@dc.tohoku.ac.jp; toshinori.kuwahara.b3@tohoku.ac.jp; shinya.fujita.a2@tohoku.ac.jp). (Corresponding author: Supakit Wattanarungsan.)

0018-9251 © 2023 IEEE

## I. INTRODUCTION

Navigation, a part guidance, navigation, and control (GNC) subsystem, is one of the most crucial subsystems of a spacecraft. Because estimation accuracy can have an enormous effect on the control performance, the attitude determination system should accurately estimate the attitude to mission requirements. The space robotic laboratory (SRL) of Tohoku University has developed many satellites since 2000, with various GNC implementations. The following are examples of the attitude navigation system of a spacecraft developed by the SRL.

RISING-2, launched in 2009, has two different attitude-control systems. A coarse attitude control system under the satellite control unit (SCU) and high precision three-axis attitude control system under an attitude control unit (ACU) are used to save power consumption from unnecessary high-accuracy attitude determination. Attitude navigation is performed using simple filters such as a low-pass filter and an average filter. It satisfied the control accuracy because there is a measurement of a high-accuracy star tracker (STT) and solar aspect sensor in the ACU [1], [2]. The model-based estimation algorithms were expected to be used in this satellite, but there was a technical problem preventing the implementation during the mission.

RISESAT, launched in 2019, with the development of the infinite impulse response (IIR) filter with a gyroscope and STT, satisfied the attitude control accuracy of  $0.1^\circ$  for Earth observation with a high-precision telescope. The IIR could reduce the randomness of the STT quaternion measurement to a certain level without statistical gain optimization, such as the Kalman filter (KF) [3], [4].

ALE-1 and ALE-2 were designed using various combinations of sensors. The static attitude determination method, tri-axial attitude determination (TRIAD) method from sun sensors and magnetometers [5], and STT measurement with an IIR filter have been implemented. Dynamic-model-based attitude determination, extended KF (EKF) with the STT and gyroscope, and angular rate integration as a backup algorithm in the case of STT measurement are unavailable [6], [7].

Furthermore, there exist many successful implementations of the EKF using measurements from sun sensors and magnetometers along with gyroscopic measurements [8], [9], [10]. These results confirm that the attitude determination EKF with gyroscopic measurement improves the estimation accuracy because it subdues the effects of environmental disturbances [11]. However, the estimator without angular rate measurement should utilize a dynamic equation, which contributes to the dynamic disturbance and disturbance torque for attitude estimation.

Because a gyroscope is the only sensor that can measure the angular rate, its failure can significantly influence the mission's success if there is no backup algorithm. Although there have been developments in microelectromechanical systems [12] and fiber-optic gyroscopes [13] that can resolve the installation limitation and extend the life of the gyroscope, attitude determination methods without a

gyroscope are still required because the survivability of these gyroscopes is still lower than that of the magnetometer. Thus, there are many studies on attitude determination without angular rate measurements. Several approaches have used STT data to estimate the angular rate by EKF [14], optimizing the process noise covariance parameter for EKF [15], or using the IIR filter, as mentioned in previous SRL satellites.

Alternatively, many approaches use magnetometer data for attitude determination, and [16], [17], [18], [19], [20], [21], [22] the advantages of using a magnetometer are listed. First, a magnetometer has the highest measurability, regardless of constraints such as lightning conditions and high angular rate conditions that star trackers and sun sensors have. Second, there is no mechanical component, which indicates high survivability. Finally, it is relatively inexpensive compared with other sensors. However, its reliability has not been tested in previous studies.

Therefore, this study aims to develop a quaternion-based EKF from magnetometer data to provide an alternative attitude determination solution for gyro-less spacecraft. EKF is designed and optimized based on the behavior of a single sensing device and the geomagnetic field. The performance is compared with the conventional magnetometer-based EKF.

The rest of this article is organized as follows. Section II discusses spacecraft dynamics and disturbance torques. Section III discusses the general attitude determination algorithm. Section IV discusses the EKF model. Section V discusses the optimization techniques and hypotheses regarding their effect on the behavior of the EKF. Section VI presents the simulation configuration, and Section VII presents the results and discussion. Finally, Section VIII concludes this article.

## II. SPACECRAFT DYNAMICS

Unlike the attitude estimation model with a gyroscope, the magnetometer-based attitude determination algorithm should estimate the angular rate. The necessary kinematic and dynamic models for EKF are discussed as follows.

The rigid-body attitude dynamic expressed in (1) propagates an angular rate and an attitude with the kinematics equation shown in (2). Environmental disturbances are also included to simulate reality

$$J\dot{\omega} = T_{\text{ctl}} + T_{\text{dtb}} - \omega \times J\omega \quad (1)$$

$$\dot{q} = \frac{1}{2} \Omega(\omega) q = \frac{1}{2} \begin{bmatrix} 0 & \omega_3 & -\omega_2 & \omega_1 \\ -\omega_3 & 0 & \omega_1 & \omega_2 \\ \omega_2 & -\omega_1 & 0 & \omega_3 \\ -\omega_1 & -\omega_2 & -\omega_3 & 0 \end{bmatrix} q \quad (2)$$

where  $J \in \mathbb{R}^{3 \times 3}$  denotes the moment of inertia tensor,  $\dot{\omega} \in \mathbb{R}^3$  denotes the time derivative of the angular rate  $\omega$ ,  $T_{\text{ctl}} \in \mathbb{R}^3$  denotes the control torque,  $T_{\text{dtb}} \in \mathbb{R}^3$  indicates the disturbance torque, and  $\dot{q} \in \mathbb{R}^4$  represents the time-derivative of the attitude quaternion  $q$ .

The following section discusses the disturbance torques that exist in LEOs.

### A. Disturbance Torques

Three disturbance sources were simulated in this study: gravity gradient, aerodynamic, and residual magnetic torques, as shown in (3). Total disturbance torque is expressed as

$$T_{\text{dtb}} = T_{\text{gg}} + T_{\text{aero}} + T_{\text{rm}} \quad (3)$$

where  $T_{\text{gg}}$ ,  $T_{\text{aero}}$ , and  $T_{\text{rm}}$  denote the gravity gradient, aerodynamic, and disturbance torques from the residual magnetic moment, respectively.

1) *Gravity Gradient Torque*: The gravity gradient torque is calculated from the summation of torques acting on each infinitesimal mass of a spacecraft owing to the gravitational force acting in the nadir direction, pointing down to the center of the Earth. Through simplification, the gravity gradient torque is expressed in terms of the moment of inertia and a nadir unit vector in the spacecraft body frame ( $n$ ) expressed as

$$T_{\text{gg}} = -\frac{3\mu}{\|r_{\text{sc}}\|^3} n \times (Jn) \quad (4)$$

where  $r_{\text{sc}}$  denotes a spacecraft's position vector from the Earth's center.  $\mu$  denotes the standard gravitational parameter of the Earth, which is equal to  $398\,400.4418 \text{ km}^3 \cdot \text{s}^{-2}$ .

2) *Aerodynamics Torque*: Aerodynamic torque is one of the most significant disturbances to spacecraft within the low-Earth orbit (LEO) and is generated from a drag force acting on each infinitesimal surface of the spacecraft. The torque acting on the spacecraft's center of mass (COM) can be calculated as follows:

$$v_{\text{rel},B} = A(q)(v + [\omega_{\oplus} \times] r_{\text{sc}}) \quad (5)$$

$$F_{\text{aero}} = -\frac{1}{2} \rho C_D \|v_{\text{rel},B}\| v_{\text{rel},B} \|S\| \cdot \max(S \cdot v_{\text{rel},B}, 0) \quad (6)$$

$$T_{\text{aero}} = \sum_{i=1}^N l^i \times F_{\text{aero}}^i \quad (7)$$

where  $A(q)$  is the direction cosine matrix from the reference to body frames of attitude  $q$ ,  $\omega_{\oplus}$  denotes an angular rate of the Earth's rotation, equal to  $7.2921158553 \times 10^{-5} \text{ rad/s}$ .  $v$  represents the spacecraft velocity in the Earth-centered inertia (ECI) frame,  $\rho$  is the atmospheric density,  $C_D$  is the drag coefficient,  $S$  is the area vector of the infinitesimal surface, and  $l^i$  represents the distance from the COM to the center of pressure.

3) *Residual Magnetic Torque*: Residual magnetic torque is caused by the residual magnetic moment of a spacecraft owing to the loop current from electrical instruments and circuits in the spacecraft following Biot–Savart's law [23]. The residual magnetic moment of the spacecraft interacts with the external magnetic field from Earth, causing an external torque expressed as follows:

$$T_{\text{rm}} = m_{\text{res}} \times b \quad (8)$$

where  $m_{\text{res}}$  denotes the residual magnetic moment, and  $b$  is the magnetic field in the body frame.

### III. ATTITUDE DETERMINATION

This section explains the derivation of the attitude determination algorithms developed in this study, discussing the relationship between observation and attitude, and the EKF structure for attitude determination.

#### A. Relationship Between Attitude and Observation

Observation models represent relationships between the observation in a reference and body frames and are used for sensing an attitude, which is expressed as

$$\begin{aligned} \mathbf{b} &= \mathbf{q} \otimes \mathbf{r} \otimes \mathbf{q}^{-1} = \mathbf{q}^{-1} \mathbf{r} \mathbf{q} \\ \mathbf{b} &= \mathbf{A}(\mathbf{q}) \mathbf{r} \end{aligned} \quad (9)$$

where  $\mathbf{b} \in \mathbb{R}^3$  denotes the measurement in the body frame and  $\mathbf{r} \in \mathbb{R}^3$  is the measurement in a reference frame: ECI frame.  $\otimes$  denotes the quaternion product operation [10] while the operation without a sign is the Hamilton product [24].

Generally, attitude determination algorithms use (9) for the observation model. However, kinematic representation observations can also be used, as observed in previous studies [16], [18], [19].

The geomagnetic field maintains its activity through the hydromagnetic dynamos of Earth [25], [26]. Therefore, its quantity changes based on the Earth-centered Earth-fixed (ECEF) frame.

The change in the magnetic field observed from the spacecraft is the contribution of the rotating spacecraft and orbital movement, expressed as

$$\dot{\mathbf{b}} = \mathbf{A}(\mathbf{q}) \dot{\mathbf{r}} - \boldsymbol{\omega} \times \mathbf{b}. \quad (10)$$

Generally, the first term is significantly smaller than the second. Therefore, this has been neglected in previous studies. However, this study considered the first term because it contains an attitude term that is useful for the attitude estimation model.

#### B. EKF for Attitude Estimation

The structure of the EKF was similar to that of a general estimator. The state of interest could not be directly measured, and the observation equation that represents the measurement and interested states was used to estimate the nonmeasurable interested states. Fig. 1 illustrates the estimator structure.

Here,  $\mathbf{m}$  represents the measurement from sensors and  $\mathbf{o}$  represents an observation that is equivalent to the estimated measurement from the estimated state.  $\mathbf{z}$  is an innovation, which is an error between measurement and observation.  $\delta\mathbf{x}$  represents the updated estimation error. The estimator in this study estimates the 6-by-1 state vector as

$$\mathbf{x} = \begin{bmatrix} \hat{\mathbf{q}} \\ \hat{\boldsymbol{\omega}} \end{bmatrix} \quad (11)$$

where variables with hat accent  $\hat{\cdot}$  are estimated variables.

EKF has two calculation steps called “update” and “propagation” with a structure, as illustrated in Fig. 1 [11].

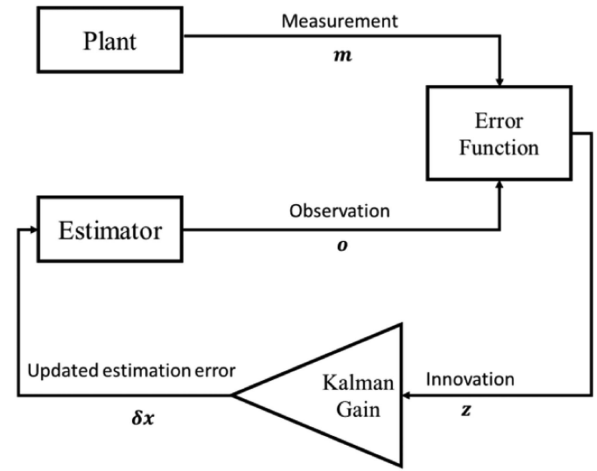


Fig. 1. Schematics of a general plant estimator.

1) *Update*: “Update” calculates Kalman and optimal gains statistically by comparing reliability between measurement and estimation and, then, updates the estimation using the following:

$$\mathbf{K} = \mathbf{P}\mathbf{H}^T\mathbf{Z}^{-1} \quad (12)$$

$$\delta\mathbf{x} = \mathbf{K}\mathbf{z} \quad (13)$$

$$\hat{\mathbf{x}}^+ = f(\hat{\mathbf{x}}^-, \delta\mathbf{x}) \quad (14)$$

where  $\mathbf{K}$  is the Kalman gain,  $\mathbf{P}$  is the estimation covariance,  $\mathbf{H}$  is the observation matrix, and  $\mathbf{Z}$  is the innovation covariance. After calculating  $\delta\mathbf{x}$ , the updated estimation  $\hat{\mathbf{x}}^+$  is performed using a function of the preupdated estimation  $\hat{\mathbf{x}}^-$  and  $\delta\mathbf{x}$ .

2) *Propagation*: “Propagation” predicts the states at the next interval based on kinematic or dynamic equations. In this study, the angular rate and quaternion were of interest, with state transition equations as follows:

$$\dot{\boldsymbol{\omega}}^{\text{true}} = \mathbf{J}^{-1} (\mathbf{T}^{\text{true}} - \boldsymbol{\omega}^{\text{true}} \times \mathbf{J}\boldsymbol{\omega}^{\text{true}}) \quad (15)$$

$$\dot{\hat{\boldsymbol{\omega}}} = \mathbf{J}^{-1} (\hat{\mathbf{T}} - \hat{\boldsymbol{\omega}} \times \mathbf{J}\hat{\boldsymbol{\omega}}) \quad (16)$$

where variables with superscript “true” are ground truth.

In this study, the spacecraft was simulated under free-spinning conditions. Therefore,  $\hat{\mathbf{T}} = [0 \ 0 \ 0]^T \text{N} \cdot \text{m}$ . Subtracting (15) and (16) to obtain the angular acceleration error  $\delta\dot{\boldsymbol{\omega}}$  as follows:

$$\begin{aligned} \delta\dot{\boldsymbol{\omega}} &= \mathbf{J}^{-1} \{ -(\hat{\boldsymbol{\omega}} + \delta\boldsymbol{\omega}) \times \mathbf{J}(\hat{\boldsymbol{\omega}} + \delta\boldsymbol{\omega}) + \hat{\boldsymbol{\omega}} \times \mathbf{J}\hat{\boldsymbol{\omega}} \} + \mathbf{T}_{\text{dtb}} \\ &= \mathbf{J}^{-1} \{ -\delta\boldsymbol{\omega} \times \mathbf{J}\hat{\boldsymbol{\omega}} - \delta\boldsymbol{\omega} \times \mathbf{J}\delta\boldsymbol{\omega} - \hat{\boldsymbol{\omega}} \times \mathbf{J}\delta\boldsymbol{\omega} \} + \mathbf{T}_{\text{dtb}}. \end{aligned} \quad (17)$$

By ignoring the second-order terms, the equation can be derived as

$$\delta\dot{\boldsymbol{\omega}} = \mathbf{J}^{-1} \{ -\delta\boldsymbol{\omega} \times \mathbf{J}\hat{\boldsymbol{\omega}} - \hat{\boldsymbol{\omega}} \times \mathbf{J}\delta\boldsymbol{\omega} \} + \mathbf{T}_{\text{dtb}}. \quad (18)$$

For quaternion, the discrete-time state transition equations are expressed as

$$\mathbf{q}_{k+1} = \Phi(\boldsymbol{\omega}_k) \mathbf{q}_k \quad (19)$$

$$\Phi(\omega_k) = \begin{bmatrix} \cos\left(\frac{1}{2}\|\omega_k\|\Delta t\right) I_3 - [\psi_k \times] & \psi_k \\ -\psi_k^T & \cos\left(\frac{1}{2}\|\omega_k\|\Delta t\right) \end{bmatrix} \quad (20)$$

$$\psi_k = \frac{\sin\left(\frac{1}{2}\|\omega_k\|\Delta t\right) \omega_k}{\|\omega_k\|} \quad (21)$$

where  $I_n \in \mathbb{R}^{n \times n}$  denotes the identity matrix, the variable with subscript  $k$  denotes a variable at the time step  $k$ ,  $\Delta t$  denotes the sampling time of the estimator, and  $[S \times]$  denotes the skew-symmetric cross-product matrix, as expressed in

$$[S \times] = \begin{bmatrix} 0 & -S_3 & S_2 \\ S_3 & 0 & -S_1 \\ -S_2 & S_1 & 0 \end{bmatrix}. \quad (22)$$

From (2), the quaternion error transition matrix can be derived using only the vector element of the quaternion as follows:

$$\delta \dot{q} = - \begin{bmatrix} \hat{\omega} \times \delta q_{1:3} \\ 0 \end{bmatrix}. \quad (23)$$

where  $\delta q$  denotes a 4-by-1 quaternion error vector and  $\delta q_{1:3}$  denotes the vector components of the quaternion error.

From (18), the discrete-time state transition matrix can be derived as follows:

$$\Phi = I_6 + F \cdot \Delta t \quad (24)$$

$$F = \begin{bmatrix} F_q & \frac{1}{2} I_3 \\ 0_{3 \times 3} & F_\omega \end{bmatrix} \quad (25)$$

$$F_q = -[\hat{\omega} \times] \quad (26)$$

$$F_\omega = \frac{\partial(\delta \dot{\omega})}{\partial(\delta \omega)} = J^{-1}\{[J\hat{\omega} \times] - [\hat{\omega} \times]J\} \quad (27)$$

where  $\Phi$  denotes the state transition matrix. From the relationships above, the covariance propagation can be expressed as follows, with the process noise covariance as:

$$P_{k+1}^- = \Phi_k P_k^+ \Phi_k^T + Q_k \quad (28)$$

where  $P_{k+1}^-$  denotes the prior estimated state error covariance at the next time step,  $P_k^+$  denotes the postestimated state error covariance at the current time step, and  $Q_k$  is the process noise covariance, which can be designed by analyzing the disturbance torque at the desired orbit and linearized propagation accuracy. Practically, the noise covariances can be online-updated following the change of uncertainty [27], but this study simplified the process of noise covariance as a constant.

#### IV. OBSERVATION MODEL DESIGN

##### A. EKF With Attitude Representation Observation (Att)

Attitude representation observation is widely used in attitude determination EKF with many combinations of sensors; however, this study only focuses on magnetometer measurements.

From (9), the innovation can be derived from the difference between the magnetic field measured in the body frame and the reference value in the ECI frame as follows:

$$z = b - A(\hat{q})r \quad (29)$$

$$b = b^{\text{true}} + v \quad (30)$$

where  $v$  denotes the magnetometer noise, which is simulated as a zero-mean Gaussian noise. According to previous studies, the innovation can be written in terms of quaternion error using the following equations with the assumption that the quaternion error is significantly smaller than the estimated quaternion [6], [7], [11], [16]:

$$A(\delta q)A(\hat{q})^T A(q^{\text{true}}) \quad (31)$$

$$A(\delta q) - I_3 = [-2\delta q \times]. \quad (32)$$

Substituting (31)–(33) into (30), respectively, the innovation becomes

$$z = b^{\text{true}} - v - A(\hat{q})r \quad (33)$$

$$z = (A(q^{\text{true}}) - A(\hat{q}))r + v \quad (34)$$

$$z = (A(\delta q)A(\hat{q}) - A(\hat{q}))r + v \quad (35)$$

$$z = [-2\delta q \times] A(\hat{q})r + v. \quad (36)$$

Rearrange the equation to extract the quaternion error as

$$z = [(2A(\hat{q})r) \times] \delta q + v. \quad (37)$$

Therefore, the observation matrix can be derived as

$$H_{\text{att}} = \begin{bmatrix} [(2A(\hat{q})r) \times] & 0_{3 \times 3} \end{bmatrix}. \quad (38)$$

The innovation covariance matrix for the EKF can be derived by calculating the expectation of innovation as

$$Z_{\text{att}} = E\{zz^T\} = H_{\text{att}} P H_{\text{att}}^T + R \quad (39)$$

where  $R$  is the measurement covariance of the magnetometer, which can be obtained by calculating the expectation of the measurement noise, considering that no correlation between the noise in each axis exists, resulting in

$$R = E\{vv^T\} = \sigma_v I_3 \quad (40)$$

where  $\sigma_v$  is the standard deviation of the magnetometer measurement noise.

Fig. 2 explains the EKF model according to the plant estimator.

##### B. EKF With Kinematics Representation Observation (Kin)

As discussed in Section II, the discrete-time derivation form was used as the secondary observation model for the EKF, as derived in (42). From this, the innovation can be derived by calculating the difference between the measurement and observation of the derivation of the magnetometer data as follows [18]:

$$\Delta \hat{b} = A(\hat{q})(r_k - r_{k-1}) + \Delta t [b_k \times] \hat{\omega}_k \quad (41)$$

$$z_k = \Delta b - \Delta \hat{b} = (b_k - b_{k-1}) - A(\hat{q})(r_k - r_{k-1}) - \Delta t [b_k \times] \hat{\omega}_k \quad (42)$$

where  $\Delta b$  denotes the difference between the magnetic field at the current time step and that at the previous time step.



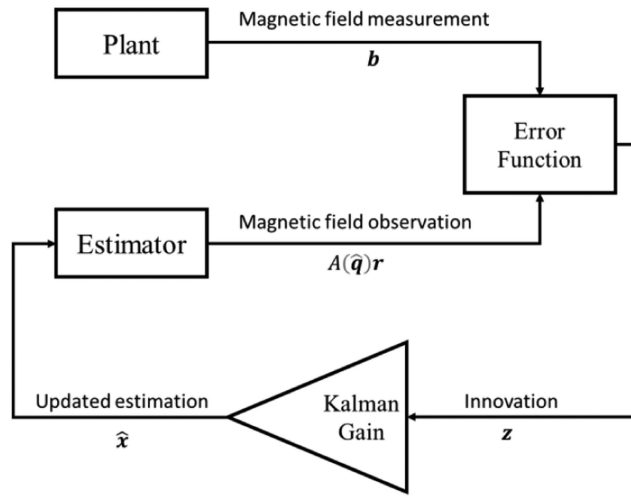


Fig. 2. Attitude representation observation EKF model diagram.

The covariance of the state estimation error can be derived by considering the following relationship:

$$\delta \omega_k = \omega_k^{\text{true}} - \hat{\omega}_k. \quad (43)$$

Substitute (31) into (43)

$$z_k = \{(b_k - b_{k-1})^{\text{true}} + (v_k - v_{k-1})\} - \{A(\hat{q})(r_k - r_{k-1}) - \Delta t [b_k \times] \hat{\omega}_k\}. \quad (44)$$

From the discretized kinematics of a rotating frame, the true magnetic field difference can be evaluated as follows:

$$(b_k - b_{k-1})^{\text{true}} = A(q_k^{\text{true}})(r_k - r_{k-1}) + \Delta t [b_k^{\text{true}} \times] \omega_k^{\text{true}} \quad (45)$$

$$(b_k - b_{k-1})^{\text{true}} = A(q_k^{\text{true}})(r_k - r_{k-1}) + \Delta t ([\hat{b}_k \times] \omega_k^{\text{true}} + [v_k \times] \hat{\omega}_k + [v_k \times] \delta \omega_k). \quad (46)$$

Neglecting the second-order term and substituting (46) into (45), the equation becomes

$$z_k = [A(q_k^{\text{true}}) - A(\hat{q}_k)](r_k - r_{k-1}) + \Delta t [\hat{b}_k \times] \times (\omega_k^{\text{true}} - \hat{\omega}_k) - \Delta t [v_k \times] \hat{\omega}_k + (v_k - v_{k-1}). \quad (47)$$

Substituting (32) into (48) yields

$$z_k = [A(\delta q_k) A(\hat{q}_k) - A(\hat{q}_k)](r_k - r_{k-1}) + \Delta t [b_k \times] \delta \omega_k - \Delta t [v_k \times] \hat{\omega}_k + (v_k - v_{k-1}). \quad (48)$$

Finally, we substitute (33) into (49) and rearrange the equation to extract the state errors. Thus, the innovation vector in terms of attitude error and rate error can be expressed as

$$z_k = [2A(\hat{q}_k)(r_k - r_{k-1}) \times] \delta q_k + \Delta t [b_k \times] \delta \omega_k - \Delta t [v_k \times] \hat{\omega}_k + (v_k - v_{k-1}). \quad (49)$$

By deriving the expectation of the innovation vector and considering there is no correlation between measurement noises, the innovation covariance can be derived as

$$Z_{\text{kin}} = H_{\text{kin}} P H_{\text{kin}}^T + 2R - \Delta t^2 [\omega \times] R [\omega \times]. \quad (50)$$

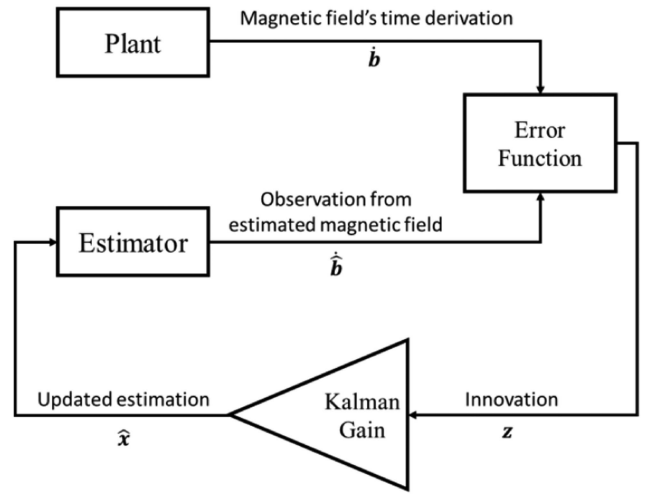


Fig. 3. Kinematics representation observation EKF model diagram.

Because the operational angular rate of the spacecraft is small, the last term can be neglected compared with the second term. Eventually, the innovation covariance becomes

$$Z_{\text{kin}} = H_{\text{kin}} P H_{\text{kin}}^T + 2R. \quad (51)$$

The observation matrix is derived as

$$H_{\text{kin}} = [[2A(\hat{q})(r_k - r_{k-1}) \times] \quad [b_k \times] \Delta t]. \quad (52)$$

The model diagram of this EKF is illustrated in Fig. 3.

### C. EKF With Combined Observation (Com)

The combined observation EKF is introduced aiming to improve the estimation accuracy and convergence of the filter. Combining the kinematic and attitude representations observation derived from prior sections, the observation matrix for the EKF can be written as

$$H = \begin{bmatrix} H_{\text{att}} \\ H_{\text{kin}} \end{bmatrix}. \quad (53)$$

The innovation vector can be derived from (30) and (43) as

$$z = \begin{bmatrix} z_{\text{att}} \\ z_{\text{kin}} \end{bmatrix}. \quad (54)$$

Similarly, the innovation covariance can be derived simply from (40) and (51) as follows:

$$Z = \begin{bmatrix} Z_{\text{att}} & 0_{3 \times 3} \\ 0_{3 \times 3} & Z_{\text{kin}} \end{bmatrix}. \quad (55)$$

## V. OPTIMIZATION METHODS

This study introduces two optimization techniques; initial state estimation and state-varying measurement covariance, as discussed in the following sections.

### A. State-Varying Measurement Covariance

Generally, every measurement contains noise, which requires statistical analysis to design the most optimal covariance. The design of the measurement covariance in this section is because the magnitude of the magnetic field

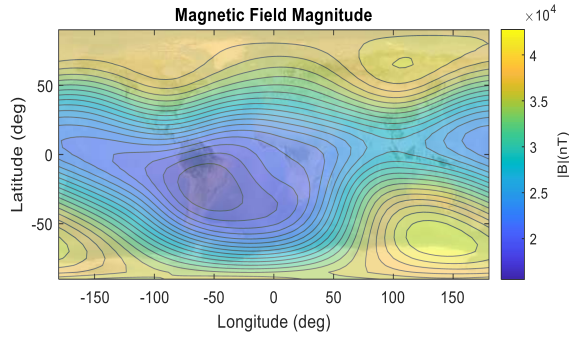


Fig. 4. Magnetic field magnitude (nanotesla) at altitude 500 km from IGRF model in the ECEF coordinate.

changes depending on the spacecraft's position, as shown in Fig. 4.

The attitude estimation algorithm uses only the directional magnetic field vector as the attitude representation. Therefore, the measurement covariance should be scaled according to the magnitude of the measured magnetic field

$$R_{\text{meas}} = \frac{R_{\text{mag}}}{r^T r} \quad (56)$$

where  $R_{\text{meas}}$  denotes the measurement covariance for the EKF and  $R_{\text{mag}}$  is the magnetometer measurement noise covariance.

### B. Initial Parameter Estimation

The static attitude determination method can be used as an initial guess for EKF. In this study, Davenport's method was used for static estimation [11], [28], [29], derived from the attitude profile matrix between measurements in the reference frame and the spacecraft's body frame as follows:

$$B \equiv \sum_{i=1}^N a_i \mathbf{b}_i \mathbf{r}_i^T \quad (57)$$

$$D = \begin{bmatrix} B + B^T - (\text{tr} B) \mathbf{I}_{3 \times 3} & \mathbf{g} \\ \mathbf{g}^T & \text{tr} B \end{bmatrix} \quad (58)$$

where  $N$  is the number of measurements,  $a_i$  is the adjustable weight,  $\text{tr} B$  is the trace of matrix  $B$ , and  $\mathbf{g}$  is calculated as follows:

$$\mathbf{g} = \sum_{i=1}^N a_i (\mathbf{b}_i \times \mathbf{r}_i) . \quad (59)$$

The attitude solution of Davenport's method is the eigenvector corresponding to the highest eigenvalue of the  $D$  matrix. In general, Davenport's method requires at least two measurements for statistical calculations [30], [31]. For magnetic field measurements, it is generally used along with sun sensors to determine the attitude solution [1], [32].

However, in this study, a magnetometer was the only sensor used for static determination. Consequently, the solution experienced singularity, as shown in Fig. 5, where several attitudes resulted in an equivalent measurement of the magnetic field from the body frame.

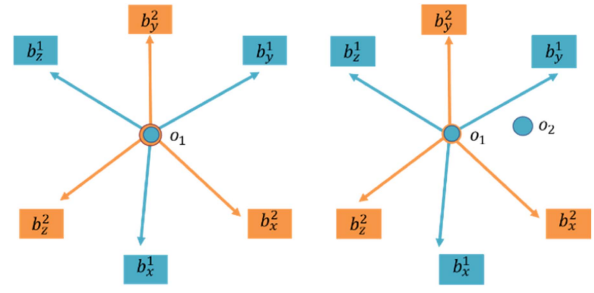


Fig. 5. Diagram of a single measurement from two different orientations (left), and a diagram of two measurements from two different orientations (right).

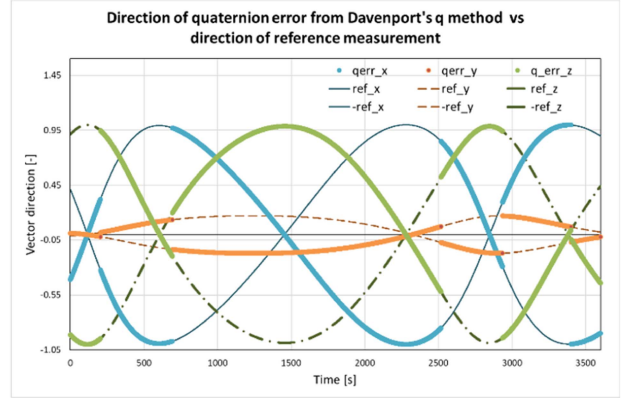


Fig. 6. Normalized attitude error from Davenport's  $q$ -method and the reference vector.

In the figure, the blue and orange coordinates represent two different orientations. A singularity occurs when only one measurement is used (left), where many solutions result in the same measurement. However, the nontrivial attitude solution can be obtained with two measurements (right) because there is only one orientation that satisfies the measurements.

Therefore, it can be hypothesized that the attitude error of this method will have the same direction as the measurement in the reference frame. To verify the hypothesis, one can compare the attitude estimation error unit vector to the magnetic field measurement, as shown in Fig. 6. From the figure, "qerr" is the normalized quaternion error, and "ref" is the normalized reference vector. This confirms the hypothesis that the quaternion error direction from Davenport's solution aligns with the magnetic field vector measured in the reference frame.

Understanding the attitude estimation error from Davenport's  $q$ -method, we can simplify the initial attitude estimation which follows Davenport's  $q$ -method as

$$\begin{aligned} \theta &= \arccos(\mathbf{b} \cdot \mathbf{r}) \\ \mathbf{q}_{1:3} &= \frac{\mathbf{b} \times \mathbf{r}}{\|\mathbf{b} \times \mathbf{r}\|} \cdot \sin\left(\frac{\theta}{2}\right) \\ q_4 &= \cos\left(\frac{\theta}{2}\right) \end{aligned} \quad (60)$$

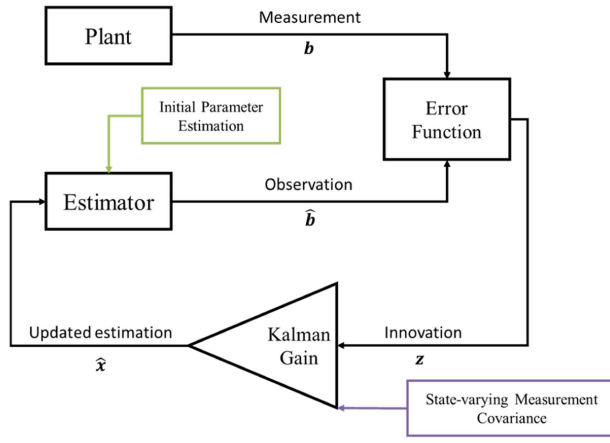


Fig. 7. Optimization techniques diagram.

which represents the shortest rotation from the reference frame. Because Davenport's  $q$ -attitude error vector aligns in the same direction as the reference vector, the attitude calculated using Davenport's  $q$ -method can initialize the EKF with the estimated initial covariance as

$$P_q^0 \equiv E\{\delta q_{1:3} \delta q_{1:3}^T\}. \quad (61)$$

According to the quaternion, a four-element vector that represents the orientation of the spacecraft is as follows:

$$q = \begin{bmatrix} q_{1:3} \\ q_4 \end{bmatrix} = \begin{bmatrix} \sin\left(\frac{\phi}{2}\right) v_{1:3} \\ \cos\left(\frac{\phi}{2}\right) \end{bmatrix} \quad (62)$$

where  $v_{1:3}$  is the rotation axis expressed in the reference frame and  $\phi$  is the amount of rotation from the reference frame.

From the singularity,  $\theta$  can take any value from 0 to  $2\pi$ . For a uniform distribution of random numbers from 0 to  $2\pi$  the standard deviation was  $\frac{2\pi}{3}$ . Thus, the initial covariance can be estimated as

$$P_q^0 \equiv E\{\delta q_{1:3} \delta q_{1:3}^T\} = \sin^2\left(\frac{\pi}{3}\right) r r^T. \quad (63)$$

Although using static estimation with only one measurement cannot calculate the correct attitude solution, it can be used as an initial estimation to avoid high innovation, which also induces a high update ratio of angular rate estimation.

In summary, the two optimization techniques involve the EKF, as depicted in Fig. 7.

## VI. SIMULATION CONFIGURATION

This study simulates the space environment in MATLAB and Simulink using the J2 perturbation gravity model and Runge–Kutta fourth-order propagation method for orbital simulation [33]. The magnetic field was generated based on the position of the spacecraft using the international geomagnetic reference field (IGRF) model [34]. Parameters for attitude determination: Magnetometer data and spacecraft position were passed through sensor models to simulate noise. The misalignment and scaled factor were neglected, assuming that they are already calibrated [11], [35], [36].

TABLE I  
Simulation Configuration

Parameter	Value	Unit
Mass ( $m$ )	10.00	[kg]
Moment of inertia ( $I$ )	$\begin{bmatrix} 0.169 & 0 & 0 \\ 0 & 0.169 & 0 \\ 0 & 0 & 0.169 \end{bmatrix}$ + 20 mm COM offset	[kg · m <sup>2</sup> ]
Initial angular velocity	Random direction with magnitude 0.2	[°/s]
Initial attitude quaternion	Randomly generated	-
Initial orbit	Pattern SSO Date 22-Mar-2022 Time 11:00:00 Position [6398, 0, 0]	- - - [km]
Magnetometer noise standard deviation	50	[nT]

TABLE II  
EKF Parameters

Parameter	Value	Unit
Magnetometer noise covariance ( $R$ )	$\begin{bmatrix} 2500 & 0 & 0 \\ 0 & 2500 & 0 \\ 0 & 0 & 2500 \end{bmatrix}$	[nT <sup>2</sup> ]
Attitude error covariance ( $Q_q$ )	$(1 \times 10^{-20})I_3$	-
Rate error covariance ( $Q_\omega$ )	$(1 \times 10^{-12})I_3$	[s <sup>-2</sup> ]
State update frequency	1	[Hz]

The spacecraft systematic parameters and estimator parameters were configured as listed in Table I. The moment of inertia in this study was the moment of inertia of a cube satellite with a 20-mm margin of the COM offset estimation error because it may affect the accuracy of the estimation practically through the error between the actual and estimated moment of inertia.

The spacecraft orbit was a sun-synchronous orbit that allows the experience of the magnetic field in various regions with different magnitudes and directions, as discussed in Section V.

The parameters related to the EKF were configured as listed in Table II. The rate error covariance was designed by the average magnitude of disturbance torque observed in

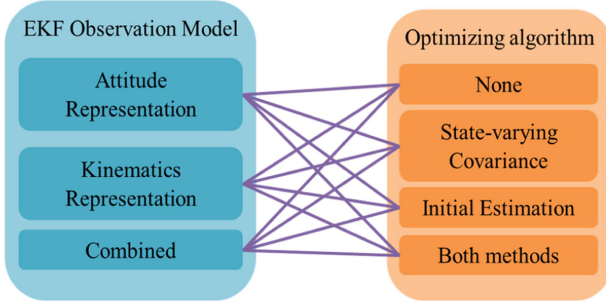


Fig. 8. Algorithm test configuration.

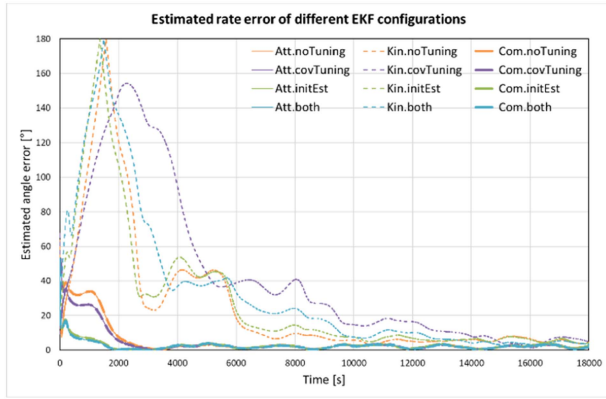


Fig. 9. Estimated angle error magnitude from the first Monte Carlo simulation case.

LEO, which is approximately  $0.1 \mu\text{N} \cdot \text{m}$  to  $1 \mu\text{N} \cdot \text{m}$ . The update frequency was set to 1 Hz.

All combinations of the proposed EKF models and optimizing algorithms were tested as configured in Fig. 8, for a total of 12 combinations.

Then, a Monte Carlo simulation of 10 different initial conditions was simulated with these combinations. The results were analyzed to study the behavior of each EKF model and confirm the hypotheses of each optimization technique.

## VII. RESULT AND DISCUSSION

The attitude and rate estimation error magnitudes from the first Monte Carlo simulation are shown in Figs. 9 and 10. The unitless innovation plots were calculated from normalized magnetic field measurements and observations.

From the figures, the first legend element indicates which EKF model was used. Att, Kin, and Com represent the attitude representation, kinematics, and combined observations, respectively. Similarly, noTuning, covTuning, initEst, and both represent the normal EKF without optimization, covariance tuning, initial estimation, and using both optimization techniques, respectively.

### A. Effect of Singularity

From Fig. 9, in the case of the Att EKF, there is a significant estimation error left until it converges after 2000 s while the innovation has already converged after 500 s, as shown in Fig. 11. This behavior is caused by singularity,

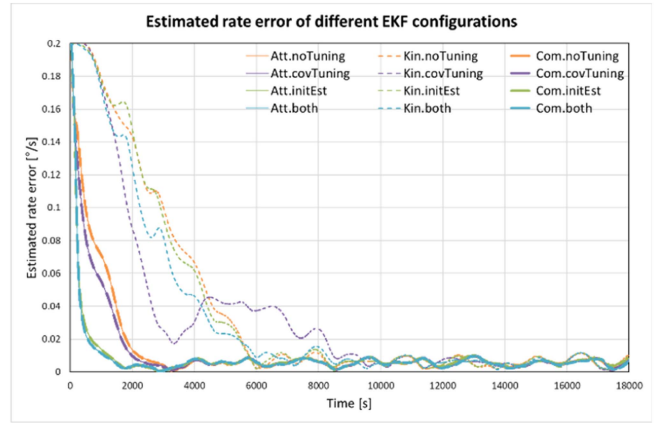


Fig. 10. Estimated rate error magnitude from the first Monte Carlo simulation case.

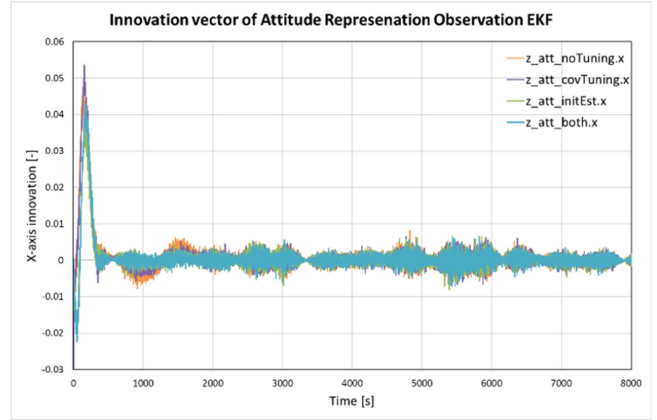


Fig. 11. Innovation vector of attitude representation observation EKF from the first Monte Carlo simulation case.

where the estimated quaternion provides a significantly small innovation, resulting in a slower convergence when compared with their estimation covariance. Particularly in a spacecraft where its motion is relatively slow, slower convergence can be observed because the EKF requires rotational motion to continue updating the estimation.

In the case of the Kin EKF shown in Fig. 12, there is little difference between the transient and steady states. This behavior can be explained by the requirement of two measurements, which introduces twice the amount of measurement noise into the innovation. Because the transient trend is unclear, we cannot conclude that the singularity is observed from the Kin EKF.

### B. EKF Model Comparison

The results indicate that Kin converges significantly more slowly than Att. This behavior means that the Kalman gain for updating Kin is smaller than Att, as calculated from the innovation covariance derived in (40) and (51), where the effective measurement covariance of Kin is at least twice that of Att. Thus, it results in slower convergence owing to smaller updates at each iteration. Consequently, the combination of the two observation models cannot help



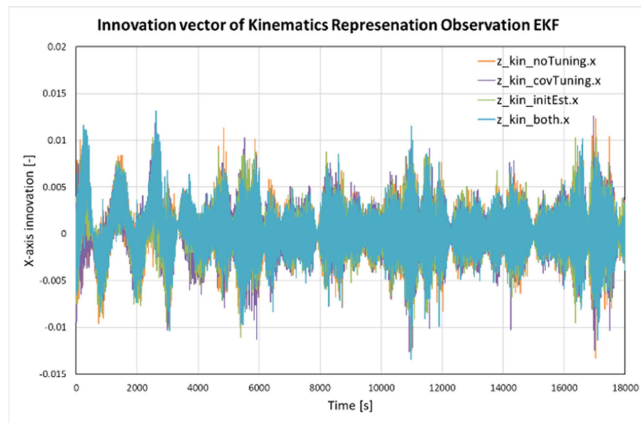


Fig. 12. Innovation vector of kinematics representation observation EKF from the first Monte Carlo simulation.

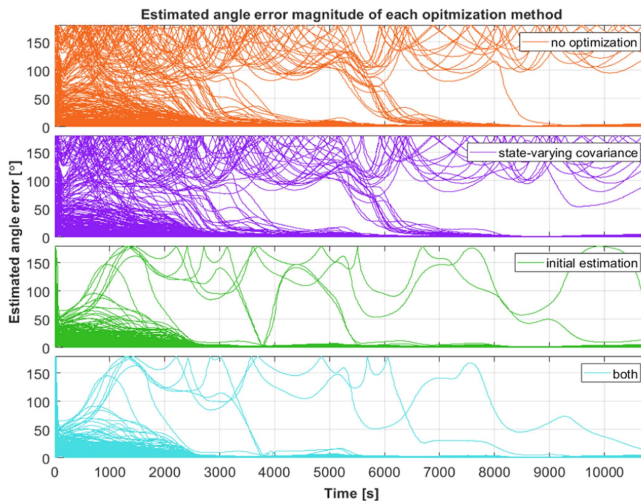


Fig. 13. Optimization-dependent attitude estimation error of attitude representation observation EKF.

avoid the singularity, as expected, because the influence of Att is much larger than that of Kin. The Kin observation model requires only one measurement, resulting in identical behavior between the Com and Att.

Therefore, the following section only discusses the results of Att EKF because the behavior of Kin EKF is significantly smaller, and the combined observation model has identical behavior compared to Att EKF.

The simulation was expanded into 200 cases and evaluated only the attitude representation observation model (Att) using different optimization techniques.

### C. Attitude Representation Observation EKF Behavior With Optimization Techniques

1) *Initial Estimation*: As shown in Fig. 14, the rate estimation error suddenly increases at the beginning in the noTuning and covTuning models. During the transient phase, the angular rate estimation error could go to approximately  $0.5^\circ/\text{s}$ , or 2.5 times above the ground truth. This indicates an aggressive response when there is a significant amount of innovation in the beginning, which causes a

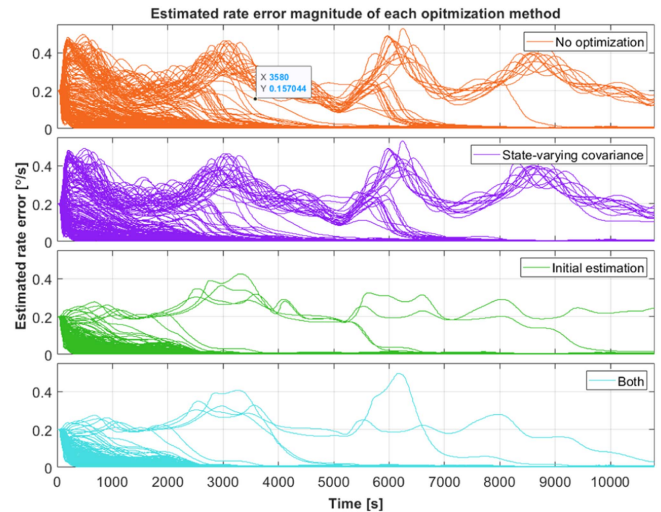


Fig. 14. Optimization-dependent rate estimation error of attitude representation observation EKF.

large update. Moreover, the innovation came from only one attitude observation that provided the shortest attitude error, which may not be the correct attitude error. This consequently affects attitude propagation, leading to slower convergence.

However, an aggressive response did not occur in the initEst and “both” models, where there was an initial estimation. This is because the method results in zero initial innovation and allows the filter to gradually update the angular rate and attitude by a residual rate error.

Thus, using the initial estimation significantly improves the behavior of the EKF, as it reduces the aggressive transient phase, which is observed in the EKF without this method.

2) *State-Varying Measurement Covariance*: As expected, the state-varying measurement covariance does not influence the accuracy once the estimation converges. However, the transient phase is slightly affected. The effect of this optimization can be observed more clearly in the kinematic representation observation, EKF (Kin).

Therefore, it can be concluded that the source of the estimation error of the magnetometer-based EKF is not the measurement process. The disturbances and estimation error of the moment of inertia contribute more significantly to the rate estimation error, which can be handled by a gyroscope in a higher accuracy estimator.

### D. Convergence

Figs. 13 and 14 show the state estimation errors from the 200-cases Monte Carlo simulation. The attitude determination accuracy was up to  $4^\circ$  with  $\sigma$  of  $0.08^\circ$ , calculated by 5-s moving average. From the results shown in Fig. 13, there are several cases from the noTuning and covTuning EKF, and two cases from the initEst EKF in which the estimation could not converge within 3 h. Because of the contribution of a non-Gaussian disturbance and singularity from using only one measurement, normal convergence determination

TABLE III  
Convergence of Each Optimization Method

Optimization method	Convergence time		Convergence percentage (%)
	Average (s)	Standard deviation (s)	
No optimization	2297	1682	95
State-varying covariance	2192	1650	94
Initial Estimation	1398	1118	99.5
Both	1368	996	100

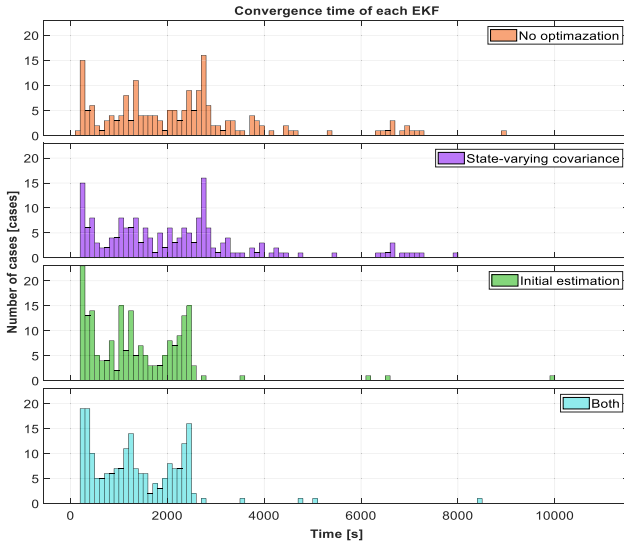


Fig. 15. Convergence time of attitude representation observation EKF with different optimization techniques from Monte Carlo Simulation.

by covariance evaluation cannot be used for this evaluation. Therefore, convergence was manually determined when the magnitude rate estimation error was maintained below  $0.02^\circ/\text{s}$  for 3 h because the filter was initiated. The convergence percentage is calculated by the number of cases that converged with a 3-h window as

$$\text{convergence percentage} = \frac{N_{\text{conv}}}{N_{\text{all}}} \quad (64)$$

where  $N_{\text{conv}}$  denotes the number of converged cases and  $N_{\text{all}}$  denotes the number of all cases, which was 200 in this study simulation. The average convergence time, its standard deviation, and the convergence percentage were calculated in Table III along with the visualized histogram of the convergence time of each case in Fig. 15.

According to the results, the EKF that uses state-varying measurement covariance has a convergence behavior similar to that of the normal EKF, with 95% convergence.

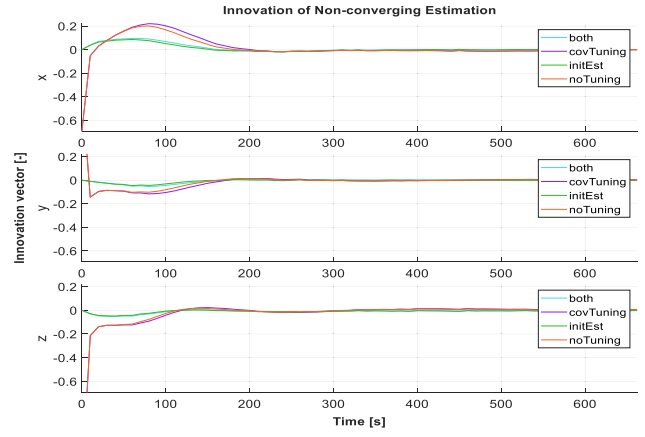


Fig. 16. Innovation of attitude representation observation EKF during the transient phase of nonconverging estimation.

Moreover, the convergence time of the normal EKF had a significantly high variance.

However, using initial estimation avoids nonconverged scenarios because it subdues an aggressive transient update from large initial innovations, resulting in 98% convergence. It also improves the reliability by reducing the distribution of the convergence time. The combination of the initial estimation and state-varying measurement covariance ensured 100% convergence.

Therefore, it can be concluded that using both optimization techniques can secure convergence, reduce convergence fluctuations, and improve convergence speed by 54%.

#### E. Innovation of the Nonconverging Estimation

Fig. 16 shows the innovation vector of the nonconverging estimation of noTuning compared with the other optimization methods during the first 600 s. While the innovations of EKFs with the initial estimation technique start at zero, other EKFs' innovations have a much larger magnitude. Fig. 17 shows the innovation vector for the entire simulation. Although the innovation of every model started to converge after 600 s, there was a relatively large quantity of residual innovations compared to the converging EKF because of incorrectly propagated states.

The direction of the estimated angular rate was approximately  $2^\circ$ – $3^\circ$  to the ground truth angular rate. However, the magnitude of the rate estimation error kept oscillating at with magnitude of  $0.25^\circ/\text{s}$ . The quaternion error maintains its direction around the magnetic field direction, which means that the estimation falls into a singularity. This behavior is caused by highly incorrect initial innovations and the nature of the EKF that the estimation covariance gradually becomes smaller at every iteration. Increasing the process noise covariance is one possible solution; however, it also results in a higher noise contribution.

#### VIII. CONCLUSION

This study investigated the magnetometer-based EKF, aiming to provide an alternative solution for spacecraft

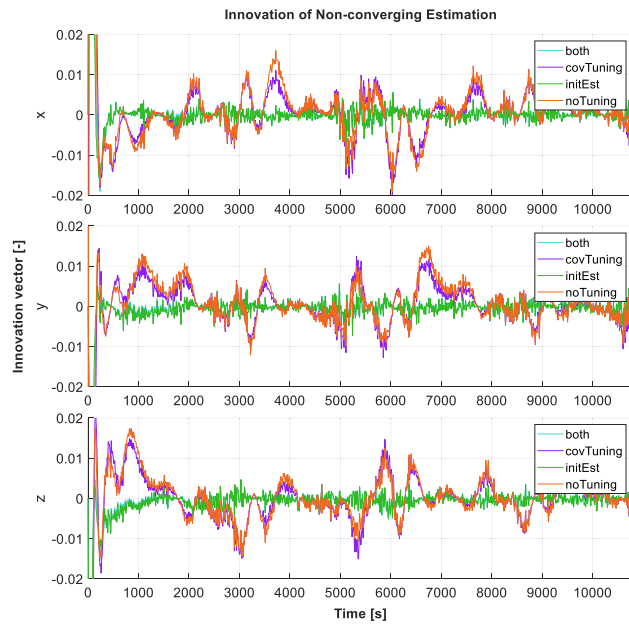


Fig. 17. Innovation of attitude representation observation EKF of nonconverging estimation (magnified).

navigation. New EKF models and optimizations were introduced in this study to improve the low reliability of the filter. The singularity is hypothesized to be a problem in the algorithm with only one sensing datum.

A Monte Carlo simulation with 200 different initial conditions was conducted to evaluate the performance of each EKF by analyzing its behavior involving the singularity by observing the innovation vector, convergence rate, and convergence time.

Based on the discussion, the kinematic representation observation EKF had fewer updates at each step, which caused the EKF with a combination of two observations to exhibit identical behavior compared to the attitude representation observation EKF.

For optimization techniques, state-varying measurements reduce the standard deviation of the convergence time but do not improve the estimation accuracy, as expected. This led to the conclusion that the accuracy of the gyroless EKF is highly dependent on disturbances and moment of inertia estimation. The initial estimation reduces aggressive behavior caused by a large magnitude of innovation, which also helps reduce convergence time and standard deviation. The combination of both techniques ensured 100% convergence based on the 200 simulation cases.

In addition, we also discovered that there existed a singularity in the steady-state phase of the filter, which was observed from a high variation of convergence time.

In summary, using the attitude representation observation EKF with both optimization techniques gives a reliable convergence and improves the convergence speed by 54% compared to the conventional algorithm. Table IV summarizes the behavior of the EKF observation model and the optimization methods.

TABLE IV  
EKF Model and Optimization Method Summary

Category	Methods	Behavior
Observation Model	Attitude Representation Observation	- Fast convergence - Singularity observed
	Kinematics Representation Observation	- Slow convergence - Larger noise contribution, cannot observe a singularity
	Combined Observation	- Dominated by Att
Optimization Method	Initial Estimation	- The fastest convergence - Significantly affect transient response
	State-varying Measurement Covariance	- No accuracy improvement - Slightly affect transient response - Combine with initial estimation improves robustness

## REFERENCES

- [1] K. Fukuda, T. Nakano, Y. Sakamoto, T. Kuwahara, K. Yoshida, and Y. Takahashi, "Attitude control system of micro satellite RISING-2," in *Proc. IEEE/SICE Int. Symp. Syst. Integration*, 2010, pp. 373–378.
- [2] K. Fukuda, N. Sugimura, Y. Sakamoto, T. Kuwahara, K. Yoshida, and Y. Takahashi, "The evaluation tests of the attitude control system of the 50-kg micro satellite RISING-2," *Trans. Jpn. Soc. Aeronaut. Space Sci. Aerosp. Technol. Jpn.*, vol. 10, no. ists28, pp. Td\_11–Td\_16, 2012.
- [3] S. Fujita, Y. Sato, T. Kuwahara, Y. Sakamoto, and K. Yoshida, "Development and ground evaluation of ground-target tracking control of microsatellite RISESAT," *Trans. Jpn. Soc. Aeronaut. Space Sci. Aerosp. Technol. Jpn.*, vol. 17, no. 2, pp. 120–126, 2019.
- [4] S. Fujita, Y. Sato, T. Kuwahara, Y. Sakamoto, and K. Yoshida, "Attitude maneuvering sequence design of high-precision ground target tracking control for multispectral Earth observations," in *Proc. IEEE/SICE Int. Symp. Syst. Integration*, 2019, pp. 153–158.
- [5] H. D. Black, "A passive system for determining the attitude of a satellite," *Amer. Inst. Aeronaut. Astronaut. J.*, vol. 2, no. 7, 1964, Art. no. 1350.
- [6] Y. Sato et al., "Establishment of the ground evaluation and operational training system of artificial meteor micro-satellite ALE-1," *Trans. Jpn. Soc. Aeronaut. Space Sci. Aerosp. Technol. Jpn.*, vol. 18, no. 3, pp. 84–92, 2020.
- [7] Y. Sato et al., "Design and evaluation of thruster control approach for micro-satellite ALE-2," in *Proc. IEEE/SICE Int. Symp. Syst. Integration*, 2020, pp. 477–482.



- [8] T. Hao, T. Kamiya, X. H. Le, S. Kawajiri, and S. Matunaga, "A reasonable and robust attitude determination and control system for nano satellite TSUBAME," in *Proc. Int. Symp. Artif. Intell., Robot. Automat. Space*, 2014.
- [9] J. Steyn, "A robust attitude measuring system for agile satellites," in *Proc. First Afr. Control Conf.*, Cape Town, Africa, 2003, pp. 444–448.
- [10] E. Lefferts, F. Marley, and M. Shuster, "Kalman filtering for spacecraft attitude estimation," *J. Guid., Control, Dyn.*, vol. 5, no. 5, pp. 417–429, 1982.
- [11] F. L. Markley and J. L. Crassidis, *Fundamentals of Spacecraft Attitude Determination and Control*. Berlin, Germany: Springer-Verlag, 2014.
- [12] B. S. Davis, "Using low-cost MEMS accelerometers and gyroscopes as strapdown IMUs on rolling projectiles," in *Proc. IEEE Position Location Navigation Symp.*, 1998, pp. 594–601.
- [13] E. J. Post, "Sagnac effect," *Rev. Modern Phys.*, vol. 39, no. 2, pp. 475–493, 1967.
- [14] P. Singla, J. Crassidis, and J. Junkins, "Spacecraft angular rate estimation algorithms for star tracker-based attitude determination," *Adv. Astronaut. Sci.*, vol. 114, pp. 1303–1316, Dec. 2003.
- [15] J. Marschke, J. Crassidis, and Q. Lam, "Attitude estimation without rate gyros using generalized multiple model adaptive estimation," in *Proc. Amer. Inst. Aeronaut. Astronaut. Guid., Navigation, Control Conf.*, 2009, Art. no. 5946.
- [16] N. Sugimura, T. Kuwahara, and K. Yoshida, "Attitude determination and control system for Nadir pointing using magnetorquer and magnetometer," in *Proc. IEEE Aerosp. Conf.*, 2016, pp. 1–12.
- [17] M. L. Psiaki, F. Martel, and P. K. Pal, "Three-axis attitude determination via Kalman filtering of magnetometer data," *J. Guid., Control, Dyn.*, vol. 13, no. 3, pp. 506–514, 1988.
- [18] P. Tortora, Y. Oshman, and F. Santoni, "Spacecraft angular rate estimation from magnetometer data only using an analytic predictor," *J. Guid., Control, Dyn.*, vol. 27, no. 3, pp. 365–373, 2004.
- [19] J. D. Searcy and H. J. Pernicka, "Magnetometer-only attitude determination using novel two-step Kalman filter approach," *J. Guid., Control, Dyn.*, vol. 35, no. 6, pp. 1693–1701, 2012.
- [20] G. A. Natanson, M. S. Challa, J. Deutschmann, and D. F. Baker, "Magnetometer-only attitude and rate determination for a gyroless spacecraft," in *Proc. 3rd Int. Symp. Space Mission Operations Ground Data Syst., Part 2*, Greenbelt, MD, USA, 1994, pp. 791–798.
- [21] S. Carletta and P. Teofilatto, "Design and numerical validation of an algorithm for the detumbling and angular rate determination of a CubeSat using only three-axis magnetometer data," *Int. J. Aerosp. Eng.*, vol. 2018, pp. 1–12, 2018.
- [22] S. Carletta, P. Teofilatto, and M. S. Farissi, "A magnetometer-only attitude determination strategy for small satellites: Design of the algorithm and hardware-in-the-loop testing," *Aerospace*, vol. 7, no. 1, pp. 1–21, 2020.
- [23] D. J. Griffiths, *Introduction of Electrodynamics*, 4th ed. Cambridge, U.K.: Cambridge Univ. Press, 2017, pp. 202–215.
- [24] W. R. Hamilton, "LXXV. On quaternions; or on a new system of imaginaries in algebra," *London, Edinburgh, Dublin Philos. Mag. J. Sci.*, vol. 31, no. 211, pp. 511–519, 1847.
- [25] A. Schekochihin, S. Cowley, J. Maron, and L. Malyskin, "Structure of small-scale magnetic fields in the kinematic dynamo theory," *Phys. Rev. E*, vol. 65, no. 1, Dec. 2002, Art. no. 016305.
- [26] N. Weiss, "Dynamoes in planets, stars and galaxies," *Astron. Geophys.*, vol. 43, no. 3, pp. 3.9–3.14, 2002.
- [27] K. Sin-Chi and Y. Ka-Veng, "Online updating and uncertainty quantification using nonstationary output-only measurement," *Mech. Syst. Signal Process.*, vol. 66, pp. 62–77, 2016.
- [28] P. B. Davenport, *A Vector Approach to the Algebra of Rotations with Applications*. Greenbelt, MD, USA: Goddard Space Flight Center, 1965.
- [29] R. Alonso and M. D. Shuster, "Complete linear attitude-independent magnetometer calibration," *J. Astronaut. Sci.*, vol. 50, no. 4, pp. 477–490, 2002.
- [30] C. C. Liebe, "Accuracy performance of star trackers-A tutorial," *IEEE Trans. Aerosp. Electron. Syst.*, vol. 38, no. 2, pp. 587–599, Apr. 2002.
- [31] T. Sun, F. Xing, X. Wang, Z. You, and D. Chu, "An accuracy measurement method for star trackers based on direct astronomic observation," *Sci. Rep.*, vol. 6, no. 1, 2016, Art. no. 22593.
- [32] F. Reichel, P. Bangert, S. Busch, K. Ravandoor, and K. Schilling, "The attitude determination and control system of the Picosatellite UWE-3\*," *Int. Federation Autom. Control Proc. Volumes*, vol. 46, no. 19, pp. 271–276, Jan. 2013.
- [33] H. D. Curtis, *Orbital Mechanics for Engineering Students*, 4th ed. Oxford, U.K.: Butterworth-Heinemann, 2021, pp. 1–54.
- [34] P. Alken et al., "International geomagnetic reference field: The thirteenth generation," *Earth Planets Space*, vol. 73, no. 1, pp. 1–25, 2021.
- [35] H. Pang et al., "Misalignment calibration of geomagnetic vector measurement system using parallelepiped frame rotation method," *J. Magnetism Magn. Mater.*, vol. 419, pp. 309–316, 2016.
- [36] M. Kok and T. B. Schön, "Magnetometer calibration using inertial sensors," *IEEE Sensors J.*, vol. 16, no. 14, pp. 5679–5689, Jul. 2016.



**Supakit Wattanarungsan** received the B.S. degree in mechanical and aerospace engineering in 2021 from Tohoku University, Sendai, Japan, where he has been working toward the M.Eng. degree in aerospace engineering since 2021.

His research interests include spacecraft attitude determination and control systems.



**Toshinori Kuwahara** (Member, IEEE) received the M.S. degree from Kyushu University, Fukuoka, Japan, in 2005, and the Dr.Eng. degree from the University of Stuttgart, Stuttgart, Germany, in 2009, both in aerospace engineering.

From 2009 to 2010, he was a Research Associate with the University of Stuttgart. From 2010 to 2015, he was an Assistant Professor, and since 2015, he has been an Associate Professor with the Department of Aerospace Engineering, Tohoku University, Sendai, Japan.

Prof. Kuwahara has been a Member of JSASS since 2010 and JSME since 2020.



**Shinya Fujita** received the B.E., M.S., and Dr. Eng. degrees in aerospace engineering from Tohoku University, Sendai, Japan, in 2014, 2016, and 2019, respectively.

Since 2019, he has been an Assistant Professor, and in 2021, he was a Senior Assistant Professor with the Department of Aerospace Engineering, Tohoku University. His research interest includes the attitude control system of microsatellites.